



The southern
stratospheric gravity
wave hot spot

N. P. Hindley et al.

This discussion paper is/has been under review for the journal Atmospheric Chemistry and Physics (ACP). Please refer to the corresponding final paper in ACP if available.

The southern stratospheric gravity-wave hot spot: individual waves and their momentum fluxes measured by COSMIC GPS-RO

N. P. Hindley, C. J. Wright, N. D. Smith, and N. J. Mitchell

Centre for Space, Atmospheric and Oceanic Sciences, University of Bath, BA2 7AY, UK

Received: 9 December 2014 – Accepted: 9 January 2015 – Published: 3 February 2015

Correspondence to: N. P. Hindley (n.hindley@bath.ac.uk)

Published by Copernicus Publications on behalf of the European Geosciences Union.

Title Page

Abstract

Introduction

Conclusions

References

Tables

Figures



Back

Close

Full Screen / Esc

Printer-friendly Version

Interactive Discussion



Abstract

During austral winter the mountains of the southern Andes and Antarctic Peninsula are a known hot spot of intense gravity wave momentum flux. There also exists a long leeward region of increased gravity wave energy that sweeps eastwards from the mountains out over the Southern Ocean, the source of which has historically proved difficult to determine. In this study we use Global Positioning System (GPS) Radio Occultation (RO) data from the Constellation Observing System for Meteorology, Ionosphere and Climate (COSMIC) satellite constellation to investigate the distribution, variability and sources of waves in the hot spot region and over the Southern Ocean. We present evidence that suggests a southward focusing of waves into the stratospheric jet from sources to the north. We also describe a wavelet analysis technique for the quantitative identification of individual waves from COSMIC temperature profiles. This analysis reveals different geographical regimes of wave amplitude and short-timescale variability in the wave field over the Southern Ocean. Finally, we take advantage of the large numbers of closely spaced pairs of profiles from the deployment phase of the COSMIC constellation in 2006 to make estimates of gravity wave horizontal wavelengths. We show that, given sufficient numbers of these pairs, GPS-RO can then produce physically reasonable estimates of stratospheric gravity wave momentum flux in the hot spot region that are consistent with other studies. The results are discussed in the context of previous satellite and modelling studies to build up a better picture of the nature and origins of waves in the southern winter stratosphere.

1 Introduction

Gravity waves are propagating mesoscale disturbances that transport energy and momentum in fluid environments. They are a vital component of the atmospheric system and a key driving mechanism in the middle and lower atmosphere through drag and diffusion processes (e.g. Fritts and Alexander, 2003, and citations therein).

ACPD

15, 3173–3217, 2015

The southern stratospheric gravity wave hot spot

N. P. Hindley et al.

Title Page

Abstract

Introduction

Conclusions

References

Tables

Figures



Back

Close

Full Screen / Esc

Printer-friendly Version

Interactive Discussion



The southern stratospheric gravity wave hot spot

N. P. Hindley et al.

Title Page

Abstract

Introduction

Conclusions

References

Tables

Figures



Back

Close

Full Screen / Esc

Printer-friendly Version

Interactive Discussion



During austral winter, the Southern Hemisphere stratosphere is home to some of the most intense gravity wave activity on Earth. At southern high-latitudes, the mountains of the southern Andes and Antarctic Peninsula are a hot spot of stratospheric gravity wave momentum flux (e.g. Ern et al., 2004; Alexander and Teitelbaum, 2007, 2011; M. J. Alexander et al., 2008). Several second-order hot spots include South Georgia (M. J. Alexander et al., 2009) and other small islands in and around the Southern Ocean (Alexander and Grimsdell, 2013; Hoffmann et al., 2013).

Accompanying the momentum flux hot spot is a long leeward distribution of increased gravity wave energy stretching eastwards from the southern Andes, Drake Passage and Antarctic Peninsula far over the Southern Ocean. This feature has puzzled researchers since it was first seen in spaceborne observations. Despite more than a decade of close observation (e.g. Wu and Waters, 1996; Wu and Jiang, 2002; Ern et al., 2004; Hei et al., 2008; M. J. Alexander et al., 2008; S. P. Alexander et al., 2009; Yan et al., 2010; Gong et al., 2012; Hendricks et al., 2014; Preusse et al., 2014) its origins are still not incontestably understood. It has been suggested that gravity waves in this region may have a number of orographic and non-orographic sources, such as the leeward propagation of mountain waves from the southern tip of South America and/or the northern tip of the Antarctic Peninsula (Preusse et al., 2002; Sato et al., 2009, 2012), baroclinic instabilities from tropospheric storm systems (Hendricks et al., 2014; Preusse et al., 2014) or spontaneous adjustment arising independently from, or as a result of, either or both of these primary processes. It is likely that the gravity waves observed in this region are a result of some or all of these processes overlapping in spatial and temporal regions. However, quantitatively identifying and describing the location, magnitude and short-timescale variability of each gravity wave source through close observation has proved exceptionally challenging. It is perhaps for this reason that the current generation of General Circulation Models (GCMs) exhibit strong disagreement in the magnitude and distribution of the flux of horizontal pseudo-momentum (henceforth referred to as momentum flux) due to gravity waves in the Southern Hemisphere stratosphere during austral winter compared to observations

(Geller et al., 2013). Particularly large discrepancies are found over the mountains of the southern Andes and Antarctic Peninsula suggesting even orographic wave drag is not simulated consistently.

For the majority of operational GCMs used in numerical weather prediction (NWP), many gravity waves are sub-gridscale phenomena and their effects must be parametrized. Parametrizations vary greatly between GCMs, but tuning parameters may for example be chosen in order to produce comparable monthly-mean zonal-mean wind fields to observations (Geller et al., 2013) or obtain a realistic quasi-biennial oscillation (QBO) (e.g. Scaife et al., 2000) while remaining physically plausible. However, a current scarcity of robust observations of key gravity wave parameters means that these parametrizations are poorly constrained (Alexander et al., 2010). With the advent of increased computing power in recent years, high spatial resolution GCMs without the need for gravity-wave parametrizations are becoming available (e.g. Watanabe et al., 2008). Such high-resolution modelling studies are promising (e.g. Sato et al., 2012), but discrepancies between observed and modelled parameters still remain. An in-depth review of the current state of gravity-wave modelling is presented by Preusse et al. (2014).

In the present study, we use Global Positioning System radio occultation (GPS-RO) data to investigate the nature and origins of waves in the southern stratospheric gravity wave hot spot and associated leeward distribution of enhanced gravity wave energy. In Sect. 2, we present maps and cross-sections of gravity wave energy in the Southern Hemisphere, with implications for oblique focussing and leeward propagation of gravity waves into the southern stratospheric jet. In Sect. 3, we present a method for the quantitative identification of individual waves from GPS-RO profiles. We use this method to investigate the geographical distribution of wave amplitudes and short-timescale variability of individual gravity waves in the wave field over the Southern Ocean. In Sect. 4, we present a method for the estimation of gravity wave momentum flux from GPS-RO measurements over the southern Andes and Antarctic Peninsula using pairs closely

The southern stratospheric gravity wave hot spot

N. P. Hindley et al.

[Title Page](#)[Abstract](#)[Introduction](#)[Conclusions](#)[References](#)[Tables](#)[Figures](#)[Back](#)[Close](#)[Full Screen / Esc](#)[Printer-friendly Version](#)[Interactive Discussion](#)

spaced and closely timed profiles. Our results are discussed in the context of other studies in Sect. 5, and in Sect. 6 the key results of the present study are summarised.

1.1 COSMIC GPS radio occultation

Launched in April 2006, The Constellation Observing System for Meteorology, Ionosphere and Climate (COSMIC) mission consists of six low Earth orbit (~ 800 km) satellites at $\sim 72^\circ$ inclination and 30° separation. A detailed description of the COSMIC constellation and the radio occultation process is provided by Liou et al. (2007). Each satellite tracks occulting GPS satellites as they rise above or set below the Earth's horizon. As the GPS signal traverses the atmospheric limb, phase delay measurements attributable to changing vertical gradients of refractivity in the atmosphere are measured. Taking an integral along the line of sight, vertical profiles of dry temperature and pressure can be computed at the tangent point of the occultation via an Abel inversion (Fjeldbo et al., 1971). The dry temperature conversion breaks down in the presence of water vapour, but works well in the stratosphere, where water vapour is negligible. Kursinski et al. (1997) estimated a temperature retrieval accuracy of ~ 0.3 K between 5–30 km, while Tsuda et al. (2011) verified multiple profiles with nearby radiosonde flights, returning discrepancies typically less than 0.5 K between 5–30 km.

In the present study we use COSMIC level 2 (version 2010.2640) post-processed dry temperature data from launch in April 2006 to the end of 2012. The sampling density of the COSMIC constellation in its final deployment configuration for a typical month in the Southern Hemisphere is shown in Fig. 1. Good coverage at high latitudes and a band of preferential sampling at around 50° S as a result of orbital geometry means that COSMIC GPS-RO is well suited to a study of the southern gravity wave hot spot and the surrounding area.

The southern stratospheric gravity wave hot spot

N. P. Hindley et al.

Title Page

Abstract

Introduction

Conclusions

References

Tables

Figures



Back

Close

Full Screen / Esc

Printer-friendly Version

Interactive Discussion



1.1.1 Vertical and horizontal resolution limits

Currently, no single observational technique can study the entire gravity wave spectrum. Each technique is sensitive to a specific portion of the gravity wave spectrum, referred to as its observational filter (Alexander and Barnet, 2007; Preusse et al., 2008; Alexander et al., 2010).

The expected vertical and horizontal resolutions of GPS-RO are discussed at length by Kursinski et al. (1997). They showed that in the stratosphere, where reasonable spherical symmetry of the local atmosphere can be assumed, the vertical resolution ΔZ of GPS-RO is primarily limited by Fresnel diffraction as

$$\Delta Z \sim 2(\lambda L_T)^{\frac{1}{2}} \quad (1)$$

where $\lambda = 19$ cm is the GPS L1 wavelength and $L_T \sim 28\,500$ km is the distance from the GPS satellite to the tangent point. From these values we find $\Delta Z \sim 1.4$ km. The vertical resolution of GPS-RO improves significantly below the tropopause due to the exponential increase of refractivity gradient with decreasing altitude, but the combination of sharp vertical temperature gradient changes, increased humidity and smaller wave amplitudes make gravity wave study in this region difficult with GPS-RO via traditional methods.

Kursinski et al. (1997) showed that the horizontal line-of-sight resolution ΔL of GPS-RO could be defined as the horizontal distance travelled by the GPS ray as it enters and exits an atmospheric layer with vertical resolution ΔZ . By a first order geometric argument, ΔL and ΔZ are approximately related as

$$\Delta L = 2(2R\Delta Z)^{\frac{1}{2}} \quad (2)$$

where R is the radius of the atmosphere at the tangent point. The horizontal line-of-sight resolution corresponding to a vertical resolution 1.4 km is ~ 270 km. Gravity waves with $\lambda_H \lesssim 270$ km in the line of sight are hence unlikely to be detected by GPS-RO. However, if the line of sight is not aligned with the wave's horizontal wavenumber vector,

The southern stratospheric gravity wave hot spot

N. P. Hindley et al.

Title Page

Abstract

Introduction

Conclusions

References

Tables

Figures



Back

Close

Full Screen / Esc

Printer-friendly Version

Interactive Discussion



the projection of λ_H in the line of sight may be longer. This means that some waves with $\lambda_H < 270$ km may be resolved. As discussed by S. P. Alexander et al. (2009), orographic waves generated by the mountains of the southern Andes and Antarctic Peninsula may tend to have roughly westward orientated horizontal wavenumber vectors, and the majority of COSMIC occultations in this region tend to be preferentially aligned towards the north–south axis. As a result, the projection of λ_H in the COSMIC line of sight is longer and the likelihood of orographic wave detection over this region is increased.

The cross-beam horizontal resolution in the stratosphere is around 1.4 km, being only diffraction limited since horizontal refractivity gradients are generally small. This is of importance to our momentum flux study in Sect. 4.

2 The gravity wave hot-spot and leeward region of increased E_p

In this section, we investigate the seasonal variability and distribution of potential energy per unit mass E_p in the Southern Hemisphere using COSMIC GPS-RO. E_p is a fundamental property of the gravity wave field and can provide a useful proxy for gravity wave activity.

In satellite observations, E_p is often derived from temperature perturbations around a background mean and can hence be calculated independently in each temperature profile. To calculate E_p , we first interpolate each dry temperature profile $T(z)$ to 100 m resolution over the altitude range 0–50 km. We obtain a background temperature profile $\bar{T}(z)$ by low-pass filtering $T(z)$ with a 2nd order Savitzky–Golay filter (Savitzky and Golay, 1964) with an 18 km frame-size and compute $T(z) - \bar{T}(z)$ to yield a temperature perturbation profile $T'(z)$.

The choice of this low-pass filter and subtraction method provides a dynamic cut-off that generally transmits features with $\lambda_z \lesssim 10$ km into our perturbation profile $T'(z)$. Transmission of vertical wavelengths longer than ~ 10 km decreases with increasing wavelength. A transmission function of this processing step is shown in Fig. 6 and discussed in more detail in Sect. 3.1. It is important to note that no digital filter can

provide a perfect cut-off in the frequency domain without introducing ringing artifacts into the spatial domain via the Gibbs phenomenon. We select the Savitzky–Golay filter as a reasonable trade-off between Gibbs ringing in the spatial domain and a sharp transition into the frequency stop band.

5 We then use $T'(z)$ and $\bar{T}(z)$ to compute $E_p(z)$ as

$$E_p(z) = \frac{1}{2} \left(\frac{g}{N} \right)^2 \left(\frac{T'(z)}{\bar{T}(z)} \right)^2 \quad (3)$$

where g is acceleration due to gravity and N is the local Brunt–Väisälä frequency. It is not meaningful to take E_p at a single height z from a single profile since a full wave cycle does not exist (S. P. Alexander et al., 2008). Hence, E_p is often taken as an
10 integral over a specified height interval when used as a proxy for gravity wave activity (e.g. Hei et al., 2008).

Unlike previous studies such as S. P. Alexander et al. (2009), no planetary wave removal techniques are applied to these data. At high latitudes, planetary waves typically have vertical scales much longer than 10 km, hence they are generally removed by our
15 filtering method. Furthermore, the long leeward distribution of enhanced gravity wave activity that we expect to see over the southern Atlantic and Indian Oceans from other studies appears morphologically similar to an $s = 1$ or part of an $s = 2$ planetary wave and may be suppressed by a Fourier or wavelet transform-based removal technique. We recognise however that some low-level planetary wave features may remain in the
20 post-processed data.

2.1 Geographic distribution of E_p in the Southern Hemisphere

Figure 2 shows E_p in the Southern Hemisphere for each month in 2010 over the height interval 26–36 km. This 10 km window generally undersamples waves with $\lambda_z > 10$ km, which further decreases the likelihood of observing planetary wave artifacts in the data.

The southern stratospheric gravity wave hot spot

N. P. Hindley et al.

Title Page

Abstract

Introduction

Conclusions

References

Tables

Figures



Back

Close

Full Screen / Esc

Printer-friendly Version

Interactive Discussion



We observe increased levels of E_p in austral winter and lower values in austral summer, consistent with other GPS-RO studies (e.g. Hei et al., 2008; S. P. Alexander et al., 2009). Between June and November, we see in Fig. 2 a long leeward region of increased E_p stretching clockwise from the Southern Andes, Drake Passage and Antarctic Peninsula at around 70° W to around 180° E. This long leeward region of increased E_p is consistent with studies using other limb sounders such as the Upper Atmosphere Research Satellite Microwave Limb Sounder (UARS-MLS) (e.g. Wu and Waters, 1996), Cryogenic Infrared Spectrometers and Telescopes for the Atmosphere (CRISTA) (e.g. Ern et al., 2004) and the High Resolution Dynamics Limb Sounder (HIRDLS) (e.g. Yan et al., 2010).

The magnitude and distribution of E_p in Fig. 2 is also consistent with results from a high-resolution modelling study by Sato et al. (2012) using the T213L256 “Kanto” GCM developed by Watanabe et al. (2008). This is significant since Sato et al. (2012) used no gravity wave parametrizations, such that all resolved waves effects were spontaneously generated. They showed a long leeward distribution of E_p at 10 hPa (~ 31 km) stretching clockwise around the southern ocean from the southern Andes and Antarctic Peninsula to around 180° W during June–October. They proposed a downwind propagation mechanism for orographic waves from the mountains of the southern Andes and Antarctic Peninsula, whereby a wave could be freely advected by the component of the mean wind perpendicular to the the wave’s horizontal wavenumber vector, and primarily attributed the long leeward distribution to this mechanism.

Some differences are apparent, however. Sato et al. (2012, their Fig. 2) showed maximum E_p directly over the mountains of the southern Andes at 10 hPa. Using data from the Atmospheric Infrared Sounder (AIRS) instrument aboard NASA’s Aqua satellite, Hendricks et al. (2014) also observed peak values directly over the mountains in a similar pattern. In our results, we see some enhancement over the mountains in the height range 26–36 km (~ 22 –5 hPa) in Fig. 2, but maximum values are usually observed well to the east. This suggests that GPS-RO is preferentially but not exclusively sensitive to the waves in the long leeward region of increased E_p out over the ocean. The ob-

The southern stratospheric gravity wave hot spot

N. P. Hindley et al.

Title Page

Abstract

Introduction

Conclusions

References

Tables

Figures



Back

Close

Full Screen / Esc

Printer-friendly Version

Interactive Discussion



servational filter of GPS-RO hence implies these waves are likely to be low-frequency inertia-gravity waves with relatively low vertical group velocities and long dwell times over the measured height range, preferentially increasing their likelihood of detection. These waves are very commonly seen in lower stratosphere observations, and can often be found far from their sources (Fritts and Alexander, 2003).

Sato et al. (2012) also observed regions of downward energy flux. In particular they found that, in the region immediately eastward of the southern tip of South America, up to 10 % of the E_p distribution consisted of downward propagating waves. This suggests that a significant portion of the E_p distribution in our results may correspond to waves that are propagating downward.

The sources of waves in the long leeward region of increased E_p are currently a topic for debate. As mentioned above, Sato et al. (2012) suggested that increased E_p over 70°W – 180°E could be primarily due to mountain waves from the southern Andes and Antarctic Peninsula that have been advected downwind, but the rest of the enhancement was likely the result of other mechanisms such as spontaneous adjustment. Other studies however suggest that much of the enhancement is primarily the result of non-orographic wave sources in and around the Southern Ocean (e.g. Hendricks et al., 2014; Preusse et al., 2014). It is thus likely that the observed distribution of E_p is the result of a number of orographic and non-orographic processes, each playing different roles in different geographical regions. In the next section we use an extended altitude range to build vertical cross-sections of stratospheric E_p in the long leeward distribution to investigate this further.

2.1.1 Vertical distribution of E_p over the southern Andes and Antarctic Peninsula

An interesting result discussed by Sato et al. (2009) and presented in Sato et al. (2012) was the apparent focusing of gravity waves into the southern stratospheric jet in the Kanto GCM. In a meridional cross-section from 30 – 70°S centred on 55°W , Sato et al. (2012, their Fig. 13) showed increased E_p values in a distinct slanted vertical column

over the southern Andes during 5 days in August. Energy flux vectors showed a large flow of energy $\sim 1500\text{--}2000$ km southward over the height region 100 hPa (~ 16 km) to 1 hPa (~ 48 km). The flow appeared to focus towards the centre of the jet, where mean zonal winds were strongest.

In our Fig. 3, we select a thin meridional cross-section of normalised monthly-mean COSMIC E_p for August 2010 centred on 65° W. This is close to the cross-section used by Sato et al. (2012). Since gravity wave amplitudes often increase with height, each height level in Fig. 3 has been normalised in order to highlight the vertical structure. Although temperature profiles from COSMIC typically exhibit increased noise above around 40 km, this normalisation and the increased number of measurements in the month-long time window potentially allow us to resolve large persistent features at higher altitudes, albeit with caution.

A slanted vertical column of increased E_p in the height region 22–35 km and a near vertical column from 35–50 km is evident in Fig. 3. The lower section of the column traverses nearly 1500 km southward over the height region 22–35 km. This suggests a clear focusing effect similar to the one suggested by Sato et al. (2012), although we cannot recover energy flux information from COSMIC. The gradient of this southward slant is greatest when the horizontal gradient in zonal wind strength is greatest, such that waves appear to be focused into the centre of the stratospheric jet. This observation is consistent with meridional ray-tracing analyses in the Kanto model (Watanabe et al., 2008; Sato et al., 2009, 2012). Above ~ 35 km however, the horizontal gradient in zonal mean wind strength is low and waves appear to generally propagate upward without further latitudinal drift.

This result suggests that waves observed at around 30–40 km over the southern tip of South America and the Drake Passage may have sources further north. In a ray-tracing analysis, Sato et al. (2012, their Fig. 5) showed that zero ground-based phase velocity waves with $\lambda_H = 300$ km launched from the southern Andes could propagate eastward and southward by up to around 2500 and 1000 km respectively in an idealized background zonal wind field. They found that waves launched from north of 45° S

The southern stratospheric gravity wave hot spot

N. P. Hindley et al.

[Title Page](#)[Abstract](#)[Introduction](#)[Conclusions](#)[References](#)[Tables](#)[Figures](#)[Back](#)[Close](#)[Full Screen / Esc](#)[Printer-friendly Version](#)[Interactive Discussion](#)

did not propagate upward due the mean wind being too weak. Our results suggest that such waves may indeed propagate from sources north of 45° S, since the slanted column in Fig. 3 is observed all the way down to 22 km over 30–45° S. This could imply that there are significant time periods where the tropospheric zonal winds are strong enough to allow vertical propagation of mountain waves from these sources.

Sato et al. (2012) also suggested that a symmetric northward focusing effect may occur for orographic waves from the Antarctic Peninsula. We investigated this using COSMIC data (not shown) and although a very slight suggestion of this effect may be evident, we could find no such clear behaviour as is observed over the southern Andes.

2.1.2 Vertical distribution of E_p over the Southern Ocean

We also investigate the vertical distribution of wave energies over the Southern Ocean. Figure 4 shows normalised E_p in a zonal cross-section centred on 50° S during August 2010. As in Fig. 3, E_p is normalised at each height level in order to highlight the vertical structure.

The vertical column of increased E_p located around 70° W in Fig. 4 is the projection in the zonal domain of the vertical column evident in Fig. 3. This column is highly suggestive of intense localised mountain wave activity from the southern Andes. The relative intensity of this column at lower altitudes suggests that, within the observational filter of COSMIC, the southern Andes is the dominant source of orographic wave activity in this latitude band. If small mountainous islands in the Southern Ocean are also significant orographic sources, as has been suggested in recent studies (M. J. Alexander et al., 2009; McLandress et al., 2012; Alexander and Grimsdell, 2013), then it is likely that waves from these islands either (1) fall outside the observation filter of GPS-RO; (2) have small amplitudes; or (3) are too intermittent over monthly time-scales to be revealed in our analysis.

The column at 70° W appears to persist over the full height range in Fig. 4. However, between 25–35 km the largest values are observed well eastward, between 60° E–60° W. These peaks are located in a deep region of increased E_p between 20–40 km

The southern stratospheric gravity wave hot spot

N. P. Hindley et al.

Title Page

Abstract

Introduction

Conclusions

References

Tables

Figures



Back

Close

Full Screen / Esc

Printer-friendly Version

Interactive Discussion



and 30°W–90°E, which is the projection in the vertical domain of the long leeward region of increased E_p seen in Fig. 2.

At first glance, Fig. 4 suggests that this long leeward region of increased E_p is strongly associated with mountain waves from the southern Andes and Antarctic Peninsula region. The lack of significant gravity wave energies upwind (westward) of the mountains and the intensity of energies downwind (eastward) is clear. As suggested by Sato et al. (2012), the increased E_p may be the result of primary mountain waves from the southern Andes and Antarctic Peninsula that have been advected downwind. However, Sato et al. (2012) also showed that waves with $\lambda_H < 350$ km rarely travelled further east than the prime meridian via this mechanism, even under ideal conditions. This suggests that it is orographic waves with $\lambda_H \gtrsim 350$ km that contribute to the region of increased E_p eastwards of the prime meridian via this advection mechanism.

It is also possible that primary orographic waves from the southern Andes and Antarctic Peninsula may contribute to the long leeward region of increased E_p then through secondary mechanisms, such as the local generation of waves in and around the stratospheric jet through breaking or other wave-mean flow interaction. The absence of significantly increased energy downwind of the Andes below 20 km in Fig. 4 indeed suggests that many of the waves present in this long leeward region of increased E_p above 20 km between 40–60°S may have been generated locally. We suspect therefore that the leeward region of increased E_p over 70°W–60°E in Fig. 4 is likely dominated by (1) primary orographic waves with $\lambda_H > 350$ km from the southern Andes or Antarctic Peninsula that have been advected downwind; and (2) and secondary waves with non-zero phase speeds generated in the breaking zones of these primary orographic waves (Bacmeister and Schoeberl, 1989). These results do not however preclude the existence of other non-orographic sources in the region, as will be discussed in Sect. 5.

The southern stratospheric gravity wave hot spot

N. P. Hindley et al.

[Title Page](#)[Abstract](#)[Introduction](#)[Conclusions](#)[References](#)[Tables](#)[Figures](#)[◀](#)[▶](#)[◀](#)[▶](#)[Back](#)[Close](#)[Full Screen / Esc](#)[Printer-friendly Version](#)[Interactive Discussion](#)

3 Individual waves

The long leeward region of increased E_p observed over the southern Atlantic and Indian Oceans is a persistent feature each year during austral winter, though some inter-annual variability exists. Multiple year averages are one way to learn about dominant processes in a region, but in order to investigate properties of a specific wave field, such as vertical wavelength or wave amplitude, a key question must first be answered: is a wave present? Once this has been answered, it becomes possible to investigate the distribution and species of individual gravity waves in a geographical region.

3.1 Wave identification (Wave-ID) methodology

This section describes the processing chain for identifying individual gravity waves from COSMIC GPS-RO temperature profiles, which is illustrated in Fig. 5. We begin by extracting temperature perturbations $T'(z)$ from each profile (Fig. 5a) as described in Sect. 2. Features with vertical scales less than ~ 2 km cannot be reliably disassociated with noise in GPS-RO temperature profiles (Marquardt and Healy, 2005). Hence, as a noise-reduction step, we apply a 2nd order Savitzky–Golay low-pass filter with a 3 km frame size to suppress these small-scale features. Note that this step has virtually no effect on vertical wavelengths greater than ~ 4 km. The transmission function of each step in this analysis is shown in Fig. 6.

Next we window the profile with a Gaussian of Full Width at Half Maximum (FWHM) 22 km centred at a height of 30 km (Fig. 5b). The purpose of this step is to focus on the height range of the profile most appropriate for gravity wave study using COSMIC GPS-RO data. This height range is chosen to generally correspond to the largest vertical region where (1) the error in bending angle is low; (2) we are unlikely to encounter spurious temperature perturbation anomalies due to incomplete background removal around the tropopause; and (3) retrieval errors associated with ionospheric effects are low (see Tsuda et al., 2011). This corresponds to a region typically between 20–40 km. The choice of a Gaussian window minimises edge effects that may arise in subsequent

Title Page

Abstract

Introduction

Conclusions

References

Tables

Figures



Back

Close

Full Screen / Esc

Printer-friendly Version

Interactive Discussion



spectral analysis. We then normalise this windowed profile such that the root-sum-square is equal to 1 (Fig. 5c).

Next, we compute the Continuous Wavelet Transform (CWT) of the normalised profile. To retain phase information, we use an 8th order complex Gaussian wavelet for the transform. Figure 5d shows squared absolute spectral amplitude of the cospectrum $|C(z, \lambda_z)|^2$.

As a result of the normalisation, the coefficients of $|C(z, \lambda_z)|^2$ in Fig. 5d can be assigned a more physical meaning. Each value represents the fractional “energy” of the profile “captured” by each wavelet at each height. Note that the term “energy” is defined as the sum-square of the values of the windowed perturbation profile and does not take any other physical meaning here. The squared absolute spectral amplitude $|C(z, \lambda_z)|^2$ is hence a confidence metric as a function of z and λ_z that represents how wave-like the transformed profile was at each height z for each vertical wavelength λ_z . High (low) values of this confidence metric imply the presence (absence) of clear wave-like features in the windowed profile. We record the maximum squared absolute spectral amplitude $C_{\max} = \max(|C(z, \lambda_z)|^2)$ located at the spectral peak.

To positively identify a wave, we require that C_{\max} exceeds a threshold value of 0.36. This choice is somewhat arbitrary, but it roughly corresponds to a wavelet “capturing” at least 60% of the root-sum-squared “energy” of the profile. If this condition is satisfied, the identification is positive and we record the vertical wavelength λ_{peak} and altitude z_{peak} at C_{\max} . As a result of the Gaussian windowing, z_{peak} is almost always located within one wavelength λ_{peak} of 30 km altitude, hence it is reasonable to consider this analysis method as sensitive to gravity waves at a height of around 30 km.

In the example in Fig. 5d, $C_{\max} \sim 0.41$ such that a wave with $\lambda_z \sim 7$ km is positively identified at an altitude near 30 km. Direct information regarding the wave’s amplitude T' is lost as a result of the CWT, so to obtain an estimate of T' we find the maximum amplitude of the temperature perturbation profile $T'(z)$ over the height region $z_{\text{peak}} \pm \lambda_{\text{peak}}/2$. In the example in Fig. 5b, $T' \sim 2.3$ K.

The southern stratospheric gravity wave hot spot

N. P. Hindley et al.

Title Page

Abstract

Introduction

Conclusions

References

Tables

Figures



Back

Close

Full Screen / Esc

Printer-friendly Version

Interactive Discussion



The southern stratospheric gravity wave hot spot

N. P. Hindley et al.

Title Page

Abstract

Introduction

Conclusions

References

Tables

Figures



Back

Close

Full Screen / Esc

Printer-friendly Version

Interactive Discussion



To summarise our requirements for a positive wave identification, we require that the wave (1) has an amplitude $1\text{ K} < T' < 10\text{ K}$; (2) has a vertical wavelength $2\text{ km} < \lambda_z < 20\text{ km}$; (3) is located such that $20\text{ km} < z_{\text{peak}} < 40\text{ km}$; and (4) has a confidence metric $C_{\text{max}} > 0.36$ as described above.

Using these criteria, we find that around 25–40 % of profiles contain an indentifiable gravity wave signal, depending on location and season. This wave identification method will be henceforth described as the Wave-ID method for convenience.

We note that this method preferentially selects profiles that contain a single large amplitude monochromatic wave with low levels of disassociated noise. A superposition of two waves of equal amplitude may result in neither being identified due to the confidence metric described above. This may also affect our amplitude estimation. However, due to phase ambiguity it is equally likely that the amplitude will increase or decrease as a result of any superposition. Hence if a sufficient number of profiles are measured, this effect should average out. Wright and Gille (2013) showed that in the Southern Hemisphere during austral winter, and particularly in the vicinity of the southern Andes and Antarctic Peninsula, there were typically fewer overlapping waves than any other geographical region. Hence, wave identification problems associated with wave superposition are likely minimised in our geographical region of interest.

The choices we have made in our Wave-ID processing will also affect the range of vertical wavelengths we detect. Figure 6 shows transmission curves as a function of wavelength for each processing step in the Wave-ID method. As shown by the net transmission curve (black solid) in Fig. 6, the combined analysis method is generally sensitive to gravity waves with $4\text{ km} < \lambda_z < 12\text{ km}$, with a sharp cut-off below 4 km and a more gradual cut-off above 12 km.

The histogram in Fig. 6 shows vertical wavelengths of gravity waves identified by this method in the region $35\text{--}75^\circ\text{ S}$ and $0\text{--}90^\circ\text{ W}$ during June–August 2006–2012. The distribution of observed vertical wavelengths generally follows the net transmission curve of synthetic waves, with peak observations at $7\text{ km} < \lambda < 9\text{ km}$.

The southern stratospheric gravity wave hot spot

N. P. Hindley et al.

Title Page

Abstract

Introduction

Conclusions

References

Tables

Figures



Back

Close

Full Screen / Esc

Printer-friendly Version

Interactive Discussion



A primary limitation of the Wave-ID method is the limited vertical window, which limits its maximum resolvable vertical wavelength. This is due to the limited vertical extent of the high-accuracy temperature retrieval of COSMIC GPS-RO. Extending the region upwards would reduce confidence in any resolved waves due to increased noise in measurements above $z \sim 38$ km (Tsuda et al., 2011). If we extend the region down much further, sharp gradients in temperature around the tropopause risk introducing spurious artifacts via traditional filtering methods (Alexander et al., 2011). Furthermore, decreasing wave amplitudes with increasing pressure in addition to the presence of water vapour makes gravity wave study below the tropopause difficult via GPS-RO. Future work may involve (1) optimising this vertical window so as to resolve the maximum possible range of vertical wavelengths; (2) investigating the optimum threshold value above which to consider a wave identification as positive; and (3) employing methods to identify overlapping waves as described by Wright and Gille (2013).

3.2 Wave identification results

In Fig. 7a we present a multi-year composite plot of E_p for June–August 2006–2012 at 30 km over the Southern Hemisphere. In this analysis, we take the mean E_p from all available profiles, including those where no significant waves are present. In Fig. 7b we produce another composite plot of E_p but calculated using only waves identified via the Wave-ID method described above. In other words, Fig. 7a is a time-averaged climatology of E_p in the region whereas Fig. 7b is the mean E_p of the waves themselves.

An initial observation is that much higher E_p values are apparent in Fig. 7b than in Fig. 7a. This is expected, since mean E_p values in Fig. 7b are skewed by the exclusion of profiles that did not contain a wave.

The same long leeward region of increased E_p sweeping around Antarctica is present in both panels of Fig. 7. The largest values in both panels are generally observed just east of the southern tip of South America and the Antarctic Peninsula, decreasing eastward and reaching a minimum just west of the Drake Passage. However, the Wave-ID method used in Fig. 7b reveals a number of differences. Firstly, the peak of the dis-

tribution of E_p in Fig. 7b resides much closer to the mountains of the southern Andes and Antarctic Peninsula. The westward shift of this peak implies that waves close to the southern Andes and Antarctic Peninsula have large amplitudes, but they are more intermittent, since this peak is diminished in the average of all available profiles. Furthermore, this peak shifts westward but the rest of the distribution remains broadly co-located with the results in Fig. 7a, which suggests that the region immediately east of the southern Andes and Antarctic Peninsula is more intermittent than the rest of the distribution. This is consistent with the hypothesis that this region is dominated by waves from orographic sources, which have been shown to be generally more intermittent than non-orographic sources in this region (Hertzog et al., 2008, 2012; Plougonven et al., 2013; Wright et al., 2013). A small enhancement is also evident at around 160° E 65° S that may be suggestive of a contribution from orographic waves from the Transantarctic Mountains.

To further investigate the nature of the wave field in this long leeward region of increased E_p , we divide the latitude band $40\text{--}65^\circ$ S into six longitudinal Sectors A–F, and examine the population of waves in each sector. Sector C contains the mountains of southern Andes, Antarctic Peninsula and South Georgia. Sector B is oceanic and upwind (westward) of these mountains. Sector D is also oceanic but immediately downwind (eastward) of the mountains. Sectors A, E and F are predominantly oceanic. Figure 9 presents histograms of individual wave amplitudes identified using the Wave-ID method in each of these six sectors during June–August 2006–2012. Note that these waves are the same used to produce the E_p distribution in Fig. 7b.

At first glance, the histograms of wave amplitudes in each sector in Fig. 9 appear broadly similar. Approximately 20 000 waves are identified in each sector and the modal amplitude is between $2\text{--}3$ K. Upon closer inspection however, some important differences become apparent.

Despite containing around 4.5 and 12 % fewer profiles than Sector B respectively, Sectors C and D contain around 13 and 6 % more identified waves respectively. This indicates that the sectors containing and immediately downwind of the southern Andes

The southern stratospheric gravity wave hot spot

N. P. Hindley et al.

[Title Page](#)[Abstract](#)[Introduction](#)[Conclusions](#)[References](#)[Tables](#)[Figures](#)[Back](#)[Close](#)[Full Screen / Esc](#)[Printer-friendly Version](#)[Interactive Discussion](#)

and Antarctic Peninsula (C, D) contain significantly more identifiable waves than sectors immediately upwind. Furthermore, Sector B has the highest number of available profiles, yet the lowest number of identified waves of any sector.

We next investigate the relative distribution of wave amplitudes in each sector compared to the zonal mean to highlight any longitudinal variation in wave amplitude populations. The rightmost panel in Fig. 9 shows the difference between the histogram in each sector and the zonal mean histogram of wave amplitudes. The curves in this panel indicate that the sectors containing and downwind of the southern Andes and Antarctic Peninsula (C, D) contain significantly more large amplitude ($3 < T' < 8$ K) waves and fewer small amplitude waves ($T' < 2.5$ K) than the zonal mean, whereas upwind Sectors A, B and F contain fewer large amplitude waves and more small amplitude waves.

Three interesting conclusions are indicated by this analysis. Firstly, the geographical region downwind (eastward) of the mountains of the southern Andes and Antarctic Peninsula up to around 40° E contains significantly more identifiable gravity waves than a region of equal size upwind (westward) of the mountains.

Secondly, this downwind region contains significantly more large amplitude waves with $3 > T' < 8$ K than the corresponding upwind region, though these large amplitude waves are still relatively rare. Since $E_p \propto (T')^2$, it is likely that the structured distribution of E_p in Fig. 7b is hence the result of an increased number of large amplitude mountain waves immediately downwind of the southern Andes and Antarctic Peninsula. In a recent study involving balloon, satellite and mesoscale numerical simulations above Antarctica and the Southern Ocean, Hertzog et al. (2012) showed that rare, large amplitude waves are not only more commonly observed above mountains in this region but that these events represent the main contribution to the total stratospheric momentum flux during the winter regime of the stratospheric circulation. Hertzog et al. (2012) also showed that gravity waves populations over open ocean tend to follow a more log-normal distribution with fewer rare, large amplitude events. Our results reinforce the findings of Hertzog et al. (2012).

The southern stratospheric gravity wave hot spot

N. P. Hindley et al.

[Title Page](#)[Abstract](#)[Introduction](#)[Conclusions](#)[References](#)[Tables](#)[Figures](#)[Back](#)[Close](#)[Full Screen / Esc](#)[Printer-friendly Version](#)[Interactive Discussion](#)

The southern stratospheric gravity wave hot spot

N. P. Hindley et al.

Title Page

Abstract

Introduction

Conclusions

References

Tables

Figures



Back

Close

Full Screen / Esc

Printer-friendly Version

Interactive Discussion



Thirdly, and perhaps most interestingly, differences in the number of identified waves and the relative distribution of wave amplitudes between sectors are significant, but relatively small in absolute terms. In general, each sector has strikingly similar distributions of wave amplitudes and total numbers of identified waves. This zonal uniformity in the distributions of wave amplitudes may be suggestive of strong, zonally uniform source mechanisms for gravity waves in all sectors, such as spontaneous adjustment or jet instability around the edge of the southern stratospheric jet. This is discussed further in Sect. 5.

4 Gravity wave momentum fluxes during JJA 2006 using COSMIC profile pairs

Gravity wave momentum flux is one of the key parameters characterising the effects of gravity waves in the atmosphere. This is of vital importance to the gravity wave modelling community, but typically difficult to obtain from observations (Fritts and Alexander, 2003; Alexander et al., 2010). Ern et al. (2004) showed that an approximation to the absolute value of momentum flux can be inferred from satellite observations of a gravity wave's amplitude T' and horizontal and vertical wavenumbers k_H and m . In the case of limb-sounding instruments such as HIRDLS and CRISTA, T' and m can be obtained directly from a single vertical temperature profile, while k_H can be estimated using the phase shift between adjacent profiles (Ern et al., 2004; M. J. Alexander et al., 2008). However, such k_H estimation methods have not routinely been applied to COSMIC, due to typically large inter-profile spacing. The scarcity of multiple profiles that are both closely spaced and closely timed with near-parallel lines of sight limits the accurate estimation of k_H in this way. Wang and Alexander (2010) investigated the use of 3 or more COSMIC profiles to make estimates of zonal and meridional horizontal wavenumbers k and l . However, as discussed by Faber et al. (2013), limitations in sampling density, aliasing and differing lines of sight restrict their approach being used in the general case.

The southern stratospheric gravity wave hot spot

N. P. Hindley et al.

Title Page

Abstract

Introduction

Conclusions

References

Tables

Figures



Back

Close

Full Screen / Esc

Printer-friendly Version

Interactive Discussion



Here we investigate an alternative approach for estimation of k_H from COSMIC GPS-RO data using a modified form of the method described by M. J. Alexander et al. (2008). We take advantage of the deployment phase of the COSMIC constellation, when pairs of satellites were often physically close (Liou et al., 2007). During this phase, a single occulting GPS satellite was often tracked by a close pair of COSMIC satellites, resulting in a significant number pairs of profiles that were closely spaced and closely timed, with near-parallel lines of sight. These particular profile pairs permit the use of a k_H estimation method and subsequently an estimation of gravity wave momentum flux. In this section, we use this method to make estimates of gravity wave momentum flux from COSMIC GPS-RO during June–August 2006 over the southern Andes, Drake Passage and Antarctic Peninsula.

4.1 Profile pair selection and processing

First, we identify profile pairs during June–August 2006 that are closely spaced, closely timed and have near-parallel lines of sight. We require that the two profiles must (1) be horizontally separated by less than 300 km at a height of 30 km; (2) be separated in time by less than 15 min; and (3) have lines of sight aligned within 30° of each other. The line of sight requirement is important since the observational filter of GPS-RO requires that waves must have $\lambda_H \gtrsim 270$ km in the line of sight. If the two viewing angles differ by a large amount, we may not resolve the same wave in both profiles. Finally, we require that a clear wave-like signal of approximately the same vertical wavelength (± 1.5 km) is identified in both profiles using the Wave-ID method described in Sect. 3.1.

In practise, we find that the majority of profile pairs during June–August 2006 have horizontal separations of 10–20 km, time separations of less than a minute and lines-of-sight separated by less than 1° . Hence requirements (1), (2) and (3) are usually satisfied. The requirement that both profiles contain the same wave-like signal reduces the number of available pairs from $\sim 21\,000$ to $\sim 7\,000$ globally during June–August 2006. Of these, around 900 lie in our geographical region of interest.

To estimate k_H in each profile pair, we follow a modified form of the method described by M. J. Alexander et al. (2008). We first apply a Gaussian window of FWHM = 22 km centred at 30 km altitude as described in Sect. 3.1. We next compute the CWT of each profile. The resulting transform $\tilde{T}(z, \lambda_z)$ is a complex valued function of altitude z and vertical wavelength λ_z . For the two profiles a and b , the cospectrum $C_{a,b}$ is computed as

$$C_{a,b} = \tilde{T}_a \tilde{T}_b^* = \hat{T}_a \hat{T}_b e^{i\Delta\phi_{a,b}} \quad (4)$$

where \hat{T} is the magnitude and $\Delta\phi_{a,b}$ is the phase difference between the two profiles for each λ_z at each position z . The covariance spectrum is the absolute value $|C_{a,b}|$. We locate the maximum in the covariance spectrum C_{\max} in the height region 20–40 km, for vertical wavelengths less than 18 km. The location of C_{\max} in the covariance spectrum corresponds to the dominant vertical wavelength λ_{DOM} common to both profiles at altitude z_{DOM} . We then compute the phase difference between the two profiles $\Delta\phi_{a,b}$ as

$$\Delta\phi_{a,b} = \arctan\left(\frac{\text{Im}(C_{a,b})}{\text{Re}(C_{a,b})}\right) \quad (5)$$

where $\text{Re}(C_{a,b})$ and $\text{Im}(C_{a,b})$ are the real and imaginary coefficients of the covariance spectrum $C_{a,b}$. We record the value of $\Delta\phi_{a,b}$ at C_{\max} .

We then compute the projection of the horizontal wavenumber k_H along the horizontal axis joining the two profiles a and b as

$$k_H = \frac{\Delta\phi_{a,b}}{\Delta r_{a,b}} \quad (6)$$

The southern stratospheric gravity wave hot spot

N. P. Hindley et al.

Title Page

Abstract

Introduction

Conclusions

References

Tables

Figures

◀

▶

◀

▶

Back

Close

Full Screen / Esc

Printer-friendly Version

Interactive Discussion



where $\Delta r_{a,b}$ is the horizontal separation of profiles a and b at around 30 km altitude. We then compute $\lambda_H = 2\pi/k_H$. This projected value of λ_H is typically longer than the true horizontal wavelength, and hence represents an upper-bound estimate (Ern et al., 2004).

To obtain an estimate of wave amplitude T' , we find the maximum amplitude in each original perturbation profile a and b over the height region $z_{\text{DOM}} \pm \lambda_{\text{DOM}}/2$, and take the mean.

Finally we compute an estimate of the absolute value of momentum flux M_{flux} as

$$M_{\text{flux}} = \frac{\bar{\rho}}{2} \frac{\lambda_z}{\lambda_H} \left(\frac{g}{N}\right)^2 \left(\frac{T'}{\bar{T}}\right)^2 \quad (7)$$

where $\bar{\rho}$ is local atmospheric density, g is acceleration due to gravity and N is the Brunt–Väisälä (buoyancy) frequency. Here, since λ_H is an upper-bound estimate, Eq. (7) represents a lower-bound estimate of gravity wave momentum flux (M. J. Alexander et al., 2008).

4.2 COSMIC momentum flux results

Figure 10 shows gravity wave vertical wavelengths, horizontal wavelengths and momentum flux from our COSMIC pair analysis over the southern Andes, Drake Passage and Antarctic Peninsula during June–August 2006. Also shown are coincident results from HIRDLS, using the Stockwell Transform (S-Transform Stockwell et al., 1996) method described by M. J. Alexander et al. (2008) modified by Wright and Gille (2013). COSMIC and HIRDLS are sensitive to different but overlapping parts of the gravity-wave spectrum, so we provide results from HIRDLS as a comparison.

In Fig. 10a, our COSMIC analysis shows longer mean vertical wavelengths over the southern tip of South America extending south over the Drake Passage. This southward extension out over the Drake Passage is in good agreement with a case study of

Title Page

Abstract

Introduction

Conclusions

References

Tables

Figures



Back

Close

Full Screen / Esc

Printer-friendly Version

Interactive Discussion



a large mountain wave event in the region by Alexander and Teitelbaum (2011), though they inferred longer vertical wavelengths due to the deep vertical weighting function of the AIRS instrument and the assumption of zero ground-based phase velocities. This region of longer vertical wavelength also extends further south over the Antarctic Peninsula.

The corresponding HIRDLS analysis in Fig. 10d shows typically longer λ_z values overall, likely due to the increased sensitivity of HIRDLS to waves with long λ_z as a result of the larger usable height range in HIRDLS profiles. Like our COSMIC analysis, Fig. 10d also shows longer mean vertical wavelengths over the southern tip of South America. However, a region of longer vertical wavelengths is also evident between 80–100° W that is not seen in our COSMIC analysis. We do not fully understand the reasons for this, but we suspect that it may be due to differing vertical wavelength sensitivities of HIRDLS and COSMIC. A full investigation into the distributions of vertical wavelengths from the HIRDLS S-Transform analysis is however beyond the scope of this study.

The results of our λ_H analysis from COSMIC profile-pairs is presented in Fig. 10b. We mostly observe values of around 600–800 km, but no structured geographical pattern is evident. We suspect this distribution may be due to the viewing geometry of GPS-RO technique, more specifically the orientation of the horizontal axis joining the two profiles in each profile pair, which can vary significantly between pairs. Since the measured horizontal wavelength is the projection of the true λ_H along the axis between the two profiles, it is an upper-bound estimate heavily dependent on the orientation of this horizontal axis. Even in a region where the wave field has a preferential horizontal alignment we will still recover a range of horizontal wavelength estimates due to differing orientations. HIRDLS scan-tracks are more consistently aligned ~NW–SE or ~NE–SW across this region, and hence estimates of λ_H between adjacent HIRDLS profiles will be more consistent, but not necessarily more accurate. This is likely the reason that the more structured geographical distribution of λ_H shown in HIRDLS re-

The southern stratospheric gravity wave hot spot

N. P. Hindley et al.

[Title Page](#)[Abstract](#)[Introduction](#)[Conclusions](#)[References](#)[Tables](#)[Figures](#)[Back](#)[Close](#)[Full Screen / Esc](#)[Printer-friendly Version](#)[Interactive Discussion](#)

sults, where shorter horizontal wavelengths are observed generally south and east of the southern tip of South America, is not observed by COSMIC.

The absolute values of our λ_H analysis are however physically reasonable and in good agreement with other studies such as Ern et al. (2004). However, our COSMIC profile-pairs typically have smaller horizontal separation (~ 20 km) between adjacent profiles than HIRDLS (~ 80 km). This means that any large positive error in phase difference $\Delta\phi_{a,b}$ between COSMIC pairs will bias our results towards shorter λ_H by the relation in Eq. (6). We suspect that this may be the reason we observe slightly lower absolute horizontal wavelength values in our COSMIC analysis than in HIRDLS. The results are not contradictory however, since both estimates represent an upper-bound.

Figure 10c shows the results of our COSMIC momentum flux analysis. Two local maxima of order 10^{-2} Pa are observed over the southern tip of South America and the Antarctic Peninsula. This increased flux over the southern tip of South America is in good agreement with results from CRISTA (Ern et al., 2004) and HIRDLS (M. J. Alexander et al., 2008) and the maximum over the Antarctic Peninsula is in good agreement with results from the Vorcore superpressure balloon campaign presented in Hertzog et al. (2008). Hertzog et al. (2008) showed that most of the momentum flux in the maximum over the Antarctic Peninsula was in a westward direction, suggestive of orographic gravity waves propagating against the mean stratospheric flow. Increased momentum flux is also observed to the east of the two maxima, suggestive of significant wakes of associated gravity wave flux downwind from these sources.

The HIRDLS analysis Fig. 10f shows a maximum over the southern tip of South America, consistent in location and magnitude with our COSMIC results. HIRDLS estimates of gravity wave momentum flux are slightly higher, but this is to be expected since HIRDLS generally resolves waves with longer λ_z . The COSMIC analysis is able to identify a secondary maximum over the Antarctic Peninsula which is not observed by HIRDLS due to the lack of measurements poleward of 62° S.

These momentum flux measurements reaffirm that the southern Andes and Antarctic Peninsula are intense and persistent sources of gravity wave momentum flux dur-

The southern stratospheric gravity wave hot spot

N. P. Hindley et al.

Title Page

Abstract

Introduction

Conclusions

References

Tables

Figures



Back

Close

Full Screen / Esc

Printer-friendly Version

Interactive Discussion



ing austral winter. Perhaps more importantly however, our results demonstrate that, given sufficient sampling density, COSMIC GPS-RO can provide physically reasonable estimates of stratospheric gravity-wave momentum flux that are consistent with results from HIRDLS, CRISTA and Vorcore. The final configuration of the COSMIC constellation however restricts the number of suitable profile-pairs such that regional climatological studies of gravity wave momentum flux using our method are generally limited to the deployment phase in 2006. However, as discussed in Sect. 5, dramatically increased sampling density provided by upcoming radio occultation missions may provide an opportunity to apply this method on a global scale in coming years.

5 Discussion

During austral winter in the Southern Hemisphere, the mountains of the southern Andes and Antarctic Peninsula are a known hot spot of gravity wave fluxes (e.g. Alexander and Teitelbaum, 2007, 2011; Hoffmann et al., 2013). However, the origin of the long leeward distribution of enhanced gravity wave energy stretching eastwards far over the ocean is currently a topic for debate.

As discussed in Sect. 2.1.2, Sato et al. (2012) suggested that waves from the mountains of the southern tip of South America and northern tip of the Antarctic Peninsula can propagate significantly downwind if their horizontal wavenumber vectors are aligned at an acute angle to the mean stratospheric flow. However, using a ray-tracing analysis Sato et al. (2012) also showed that for horizontal wavelengths of 250–350 km such waves rarely propagate east of the prime meridian, regardless of launch angle. Hence, the distribution of increased E_p shown here eastwards of around 20° E is not likely to be explained by the downwind propagation of waves with λ_H less than approximately 350 km. This suggests that the distribution of increased E_p eastwards of around 20° E may be the result of (1) downwind propagating mountain waves with $\lambda_H > 350$ km; (2) locally generated non-orographic waves from tropospheric or stratospheric sources out over the ocean; or (3) some combination of these processes.

The southern stratospheric gravity wave hot spot

N. P. Hindley et al.

Title Page

Abstract

Introduction

Conclusions

References

Tables

Figures



Back

Close

Full Screen / Esc

Printer-friendly Version

Interactive Discussion



The southern stratospheric gravity wave hot spot

N. P. Hindley et al.

Title Page

Abstract

Introduction

Conclusions

References

Tables

Figures



Back

Close

Full Screen / Esc

Printer-friendly Version

Interactive Discussion



Preusse et al. (2014) used backwards ray-tracing of resolved waves in ECMWF data to show that during August 2008, waves over the southern Andes and Antarctic Peninsula overwhelmingly had lowest traceable altitude (LTA) values close to the surface, whereas waves over the southern Atlantic and Indian oceans often had average LTA values around 7–12 km. Their results are indicative of upper-tropospheric non-orographic wave sources that exist out over the oceans. Similarly, Hendricks et al. (2014) suggested that a belt of increased stratospheric gravity wave activity observed by AIRS could be attributed to non-orographic sources in winter storm tracks around the southern Atlantic and Indian Oceans. Our results presented in Figs. 3 and 4 are not strongly suggestive of intense tropospheric non-orographic wave sources over the oceans, although these results do not explicitly preclude the existence of such sources. Furthermore, the waves considered by Preusse et al. (2014) are typically below the height region considered in this study, and the waves observed by Hendricks et al. (2014) are not typically visible to GPS-RO. We note, however, that the processes they describe may indeed have an influence on the distribution of E_p that we observe in COSMIC data.

In Sect. 2.1.1 we presented evidence of a southward focussing of gravity waves into the centre of the stratospheric jet. In a recent modelling study, McLandress et al. (2012) showed that zonal wind biases and vortex breakdown timing errors in a latitude band near 60° S could be greatly reduced in the Canadian Middle Atmosphere Model (CMAM) through the inclusion of non-specific orographic gravity wave drag (GWD) in the stratosphere. One hypothesis for the missing drag is unparametrized mountain waves from small islands in and around the Southern Ocean that are sub-gridscale in CMAM. A second hypothesis is the southward (northward) propagation of orographic waves from the north (south) into the southern stratospheric jet from outside the latitude band. Our results provide evidence of such meridional propagation. In particular, we observe a southward focusing of waves in Fig. 3 into the jet around 60° W from sources further north, supporting the second hypothesis of McLandress et al. (2012) described above. It is conceivable that there exists a similar process whereby waves

from the Antarctic Peninsula are focussed northwards into the jet, though we are unable to find such clear evidence for this in our results. Observational evidence of any meridional focusing is significant since many parametrization schemes used operationally in GCMs do not include such focussing phenomena (Preusse et al., 2014).

In Sect. 3 we investigated longitudinal variations in wave populations in the long leeward region of increased E_p during June–August 2006–2012. In regions immediately downwind of the southern Andes and Antarctic Peninsula we observe significantly more rare, large amplitude waves than in upwind regions, while only a slight increase in the absolute number of waves is observed. Further analysis (omitted for brevity) showed that exclusion of these large amplitude waves resulted in a much more zonally uniform distribution of mean wave energy around over the Southern Ocean. This suggests that the increased E_p observed immediately downwind of the mountains in Fig. 7b is the result of increased numbers of rare, large amplitude wave events in this downwind region and not simply the result of more waves in general. As discussed in Sect. 3.2, this is consistent with the results of a super-pressure balloon and modelling study by Hertzog et al. (2012). The eastward decrease in E_p values in Fig. 7b correlates well to the eastward decrease of the frequency of occurrence of these rare, large amplitudes waves.

However, the general distributions of gravity wave amplitudes at all longitudes in the latitude band 40–65° S are broadly similar. This may be indicative of persistent, zonally uniform non-orographic source mechanisms in and around the stratospheric jet. Inertia-gravity waves, to which GPS-RO is preferentially sensitive, can often be generated at the edge of jet streams via spontaneous adjustment processes (Fritts and Alexander, 2003). Hence, a significant contribution to the long leeward region of increased E_p in Fig. 7b may be from gravity waves generated via these adjustment mechanisms.

In the context of other studies, our results therefore suggest that the long leeward region of increased E_p consists of (1) rare, large amplitude waves over 80° W–40° E from orographic sources such as the southern Andes and Antarctic Peninsula that have been focussed and advected downwind; (2) secondary waves generated locally in the

The southern stratospheric gravity wave hot spot

N. P. Hindley et al.

[Title Page](#)[Abstract](#)[Introduction](#)[Conclusions](#)[References](#)[Tables](#)[Figures](#)[Back](#)[Close](#)[Full Screen / Esc](#)[Printer-friendly Version](#)[Interactive Discussion](#)

breaking region of these primary orographic waves; and (3) a zonally uniform distribution of small amplitude waves from non-orographic mechanisms such as spontaneous adjustment and jet instability around the edge of the stratospheric jet. A contribution from tropospheric non-orographic waves associated with storms around the southern Atlantic and Indian Oceans may also be present.

Finally, we described a method for the estimation of stratospheric gravity wave momentum flux from COSMIC GPS-RO. To our knowledge, there are very few studies that have successfully developed methodologies for gravity wave momentum flux estimates from GPS-RO data (e.g. Wang and Alexander, 2010). Our results demonstrate that, given sufficient sampling density, COSMIC GPS-RO can produce physically reasonable estimates of stratospheric gravity wave momentum flux over the southern Andes and Antarctic Peninsula that are consistent with results from CRISTA, HIRDLS and Vorcore (Ern et al., 2004; M. J. Alexander et al., 2008; Hertzog et al., 2008).

The method presented here is mostly limited to the deployment phase of the COSMIC constellation only, since the number of profile-pairs that satisfy the requirements outlined in Sect. 4.1 is very low once the satellites reached their final configuration.

However, GPS-RO is an expanding technique, with new missions scheduled for launch in the next decade. The 12-satellite COSMIC-2 constellation (Cook et al., 2013) will boast more than 8000 soundings per day, measuring the occultations of satellites from the European navigation satellite system GALILEO and the Russian Global Navigation Satellite System (GLONASS), in addition to the American GPS satellite constellation. COSMIC-2 will feature two deployment phases from which large numbers of closely spaced profile-pairs can be expected. Furthermore, the number of profile-pairs available from their final configuration is likely to increase significantly and there will be increased coverage in the tropics as a result of 6 low-inclination (24°) satellites.

The southern stratospheric gravity wave hot spot

N. P. Hindley et al.

[Title Page](#)[Abstract](#)[Introduction](#)[Conclusions](#)[References](#)[Tables](#)[Figures](#)[Back](#)[Close](#)[Full Screen / Esc](#)[Printer-friendly Version](#)[Interactive Discussion](#)

6 Summary

In the present study we use dry atmospheric temperature profiles from COSMIC GPS-RO to investigate gravity wave activity in the southern stratospheric hot spot around the southern Andes and Antarctic Peninsula. We also investigate the long leeward region of increased E_p stretching out over the southern oceans during austral winter. In the hot spot region, we present evidence that indicates a southward focusing of orographic gravity waves into the strong winds of the southern stratospheric jet. These waves appear to come from sources far to the north during August 2010. This phenomenon has been predicted by recent high-resolution modelling studies (e.g. Watanabe et al., 2008; Sato et al., 2009, 2012).

Our results, in the context of other studies, suggest that the long leeward region of increased E_p is the result of waves from a number of overlapping orographic and non-orographic wave sources.

Large mean E_p values observed immediately downwind of the southern Andes and Antarctic Peninsula are attributed to an increased number of rare, large amplitude mountain waves that have propagated downwind via the mechanism described by Sato et al. (2012). The remaining distribution is likely the result of waves from a variety of non-orographic sources such as storms in and around the Southern Ocean (Hendricks et al., 2014; Preusse et al., 2014) and spontaneous adjustment mechanisms around the edge of the southern stratospheric jet (Fritts and Alexander, 2003; Hei et al., 2008).

We also describe a method for the estimation of k_H from closely spaced pairs of COSMIC profiles during the deployment phase of the constellation in July–August 2006. We show that, given sufficient sampling density, estimations of gravity wave momentum flux in the region around the southern Andes and Antarctic Peninsula can be retrieved from COSMIC GPS-RO. These measurements are broadly consistent with results from CRISTA (Ern et al., 2004), HIRDLS (M. J. Alexander et al., 2008), and Vorcore (Hertzog et al., 2008). In the coming years, the increased sampling den-

The southern stratospheric gravity wave hot spot

N. P. Hindley et al.

Title Page

Abstract

Introduction

Conclusions

References

Tables

Figures



Back

Close

Full Screen / Esc

Printer-friendly Version

Interactive Discussion



sity offered by new GPS-RO missions may allow our approach to be temporally and geographically expanded, potentially providing estimates of stratospheric gravity wave momentum flux on a much wider scale.

Acknowledgements. This study is generously supported by the UK Natural Environment Research Council (NERC). We are grateful to Andrew Moss for helpful suggestions and discussions. We would also like to acknowledge Harrower and Brewer (2003) for the ColorBrewer colormaps featured in this study.

References

- Alexander, M. J. and Barnett, C.: Using satellite observations to constrain parameterizations of gravity wave effects for global models, *J. Atmos. Sci.*, 64, 1652–1665, doi:10.1175/JAS3897.1, 2007. 3178
- Alexander, M. J. and Grimsdell, A. W.: Seasonal cycle of orographic gravity wave occurrence above small islands in the Southern Hemisphere: implications for effects on the general circulation, *J. Geophys. Res.*, 118, 11589–11599, doi:10.1002/2013JD020526, 2013. 3175, 3184
- Alexander, M. J. and Teitelbaum, H.: Observation and analysis of a large amplitude mountain wave event over the Antarctic peninsula, *J. Geophys. Res.*, 112, D21103, doi:10.1029/2006JD008368, 2007. 3175, 3198
- Alexander, M. J. and Teitelbaum, H.: Three-dimensional properties of Andes mountain waves observed by satellite: a case study, *J. Geophys. Res.*, 116, D23110, doi:10.1029/2011JD016151, 2011. 3175, 3196, 3198
- Alexander, M. J., Gille, J., Cavanaugh, C., Coffey, M., Craig, C., Eden, T., Francis, G., Halvorson, C., Hannigan, J., Khosravi, R., Kinnison, D., Lee, H., Massie, S., Nardi, B., Barnett, J., Hepplewhite, C., Lambert, A., and Dean, V.: Global estimates of gravity wave momentum flux from High Resolution Dynamics Limb Sounder observations, *J. Geophys. Res.*, 113, D15S18, doi:10.1029/2007JD008807, 2008. 3175, 3192, 3193, 3194, 3195, 3197, 3201, 3202
- Alexander, M. J., Eckermann, S. D., Broutman, D., and Ma, J.: Momentum flux estimates for South Georgia Island mountain waves in the stratosphere observed via satellite, *Geophys. Res. Lett.*, 36, L12816, doi:10.1029/2009GL038587, 2009. 3175, 3184

The southern stratospheric gravity wave hot spot

N. P. Hindley et al.

Title Page

Abstract

Introduction

Conclusions

References

Tables

Figures



Back

Close

Full Screen / Esc

Printer-friendly Version

Interactive Discussion



The southern stratospheric gravity wave hot spot

N. P. Hindley et al.

Title Page

Abstract

Introduction

Conclusions

References

Tables

Figures



Back

Close

Full Screen / Esc

Printer-friendly Version

Interactive Discussion



- Alexander, M. J., Geller, M., McLandress, C., Polavarapu, S., Preusse, P., Sassi, F., Sato, K., Eckermann, S., Ern, M., Hertzog, A., Kawatani, Y., Pulido, M., Shaw, T., Sigmond, M., Vincent, R., and Watanabe, S.: Recent developments in gravity-wave effects in climate models and the global distribution of gravity-wave momentum flux from observations and models, Q. J. Roy. Meteor. Soc., 136, 1103–1124, doi:10.1002/qj.637, 2010. 3176, 3178, 3192
- Alexander, P., de la Torre, A., Llamedo, P., Hierro, R., Schmidt, T., Haser, A., and Wickert, J.: A method to improve the determination of wave perturbations close to the tropopause by using a digital filter, Atmos. Meas. Tech., 4, 1777–1784, doi:10.5194/amt-4-1777-2011, 2011. 3189
- Alexander, S. P., Tsuda, T., Kawatani, Y., and Takahashi, M.: Global distribution of atmospheric waves in the equatorial upper troposphere and lower stratosphere: COSMIC observations of wave mean flow interactions, J. Geophys. Res., 113, D24115, doi:10.1029/2008JD010039, 2008. 3180
- Alexander, S. P., Klekociuk, A. R., and Tsuda, T.: Gravity wave and orographic wave activity observed around the Antarctic and Arctic stratospheric vortices by the COSMIC GPS-RO satellite constellation, J. Geophys. Res., 114, D17103, doi:10.1029/2009JD011851, 2009. 3175, 3179, 3180, 3181
- Bacmeister, J. T. and Schoeberl, M. R.: Breakdown of vertically propagating two-dimensional gravity waves forced by orography, J. Atmos. Sci., 46, 2109–2134, 1989. 3185
- Cook, K., Fong, C. J., Yen, N., Wenkel, M. J., Wilezynski, P., and Chang, G. S.: FORMOSAT-7/COSMIC-2 GNSS radio occultation constellation mission for global weather monitoring, IEEE Aerospace Conference, Big Sky, MT, 2–9 March 2013, 1–8, doi:10.1109/AERO.2013.6497317, 2013. 3201
- Ern, M., Preusse, P., Alexander, M. J., and Warner, C. D.: Absolute values of gravity wave momentum flux derived from satellite data, J. Geophys. Res., 109, D20103, doi:10.1029/2004JD004752, 2004. 3175, 3181, 3192, 3195, 3197, 3201, 3202
- Faber, A., Llamedo, P., Schmidt, T., de la Torre, A., and Wickert, J.: On the determination of gravity wave momentum flux from GPS radio occultation data, Atmos. Meas. Tech., 6, 3169–3180, doi:10.5194/amt-6-3169-2013, 2013. 3192
- Fjeldbo, G., Kliore, A. J., and Eshleman, V. R.: The neutral atmosphere of Venus as studied with the Mariner V radio occultation experiments, Astron. J., 76, 123–140, doi:10.1086/111096, 1971. 3177
- Fritts, D. C. and Alexander, M. J.: Gravity wave dynamics and effects in the middle atmosphere, Rev. Geophys., 41, 1003, doi:10.1029/2001RG000106, 2003. 3174, 3182, 3192, 3200, 3202

The southern stratospheric gravity wave hot spot

N. P. Hindley et al.

Title Page

Abstract

Introduction

Conclusions

References

Tables

Figures



Back

Close

Full Screen / Esc

Printer-friendly Version

Interactive Discussion



Geller, M., Alexander, M. J., Love, P., Bacmeister, J., Ern, M., Hertzog, A., Manzini, E., Preusse, P., Sato, K., Scaife, A., and Zhou, T.: A comparison between gravity wave momentum fluxes in observations and climate models, *J. Climate*, 26, 6383–6405, doi:10.1175/JCLI-D-12-00545.1, 2013. 3176

5 Gong, J., Wu, D. L., and Eckermann, S. D.: Gravity wave variances and propagation derived from AIRS radiances, *Atmos. Chem. Phys.*, 12, 1701–1720, doi:10.5194/acp-12-1701-2012, 2012. 3175

Harrower, M. and Brewer, C.: ColorBrewer.org: an online tool for selecting colour schemes for maps, *Cartogr. J.*, 40, 27–37, doi:10.1179/000870403235002042, 2003. 3203

10 Hei, H., Tsuda, T., and Hirooka, T.: Characteristics of atmospheric gravity wave activity in the polar regions revealed by GPS radio occultation data with CHAMP, *J. Geophys. Res.*, 113, D04107, doi:10.1029/2007JD008938, 2008. 3175, 3180, 3181, 3202

Hendricks, E., Doyle, J., Eckermann, S. D., Jiang, Q., and Reinecke, P.: What is the source of the stratospheric gravity wave belt in austral winter?, *J. Atmos. Sci.*, 71, 1583–1592, doi:10.1175/JAS-D-13-0332.1, 2014. 3175, 3181, 3182, 3199, 3202

15 Hertzog, A., Boccara, G., Vincent, R. A., Vial, F., and Cocquerez, P.: Estimation of gravity wave momentum flux and phase speeds from quasi-Lagrangian stratospheric balloon flights. Part II: Results from the Vorcore campaign in Antarctica., *J. Atmos. Sci.*, 65, 3056–3070, doi:10.1175/2008JAS2710.1, 2008. 3190, 3197, 3201, 3202

20 Hertzog, A., Alexander, M. J., and Plougonven, R.: On the intermittency of gravity wave momentum flux in the stratosphere, *J. Atmos. Sci.*, 69, 3433–3448, doi:10.1175/JAS-D-12-09.1, 2012. 3190, 3191, 3200

Hoffmann, L., Xue, X., and Alexander, M. J.: A global view of stratospheric gravity wave hotspots located with Atmospheric Infrared Sounder observations, *J. Geophys. Res.-Atmos.*, 118, 416–434, doi:10.1029/2012JD018658, 2013. 3175, 3198

25 Kursinski, E. R., Hajj, G. A., Schofield, J. T., Linfield, R. P., and Hardy, K. R.: Observing Earth's atmosphere with radio occultation measurements using the Global Positioning System, *J. Geophys. Res.*, 102, 23429–23465, doi:10.1029/97JD01569, 1997. 3177, 3178

30 Liou, Y. A., Pavelyev, A. G., Pavelyev, A. A., Yen, N., Huang, C. Y., and Fong, C. J.: FORMOSAT-3/COSMIC GPS radio occultation mission: preliminary results, *IEEE T. Geosci. Remote*, 45, 3813–3826, 2007. 3177, 3193

The southern stratospheric gravity wave hot spot

N. P. Hindley et al.

Title Page

Abstract

Introduction

Conclusions

References

Tables

Figures



Back

Close

Full Screen / Esc

Printer-friendly Version

Interactive Discussion



- Marquardt, C. and Healy, S. B.: Measurement noise and stratospheric gravity wave characteristics obtained from GPS occultation data, *J. Meteorol. Soc. Jpn.*, 83, 417–428, doi:10.2151/jmsj.83.417, 2005. 3186
- McLandress, C., Shepherd, T. G., Polavarapu, S., and Beagley, S. R.: Is missing orographic gravity wave drag near 60° S the cause of the stratospheric zonal wind biases in chemistry–climate models?, *J. Atmos. Sci.*, 69, 802–818, doi:10.1175/JAS-D-11-0159.1, 2012. 3184, 3199
- Plougonven, R., Hertzog, A., and Guez, L.: Gravity waves over Antarctica and the Southern Ocean: consistent momentum fluxes in mesoscale simulations and stratospheric balloon observations, *Q. J. Roy. Meteor. Soc.*, 139, 101–118, doi:10.1002/qj.1965, 2013. 3190
- Preusse, P., Doernbrack, A., and Eckermann, S.: Space-based measurements of stratospheric mountain waves by CRISTA 1. Sensitivity, analysis method, and a case study, *J. Geophys. Res.*, 107, 8178, doi:10.1029/2001JD000699, 2002. 3175
- Preusse, P., Eckermann, S. D., and Ern, M.: Transparency of the atmosphere to short horizontal wavelength gravity waves, *J. Geophys. Res.*, 113, D24104, doi:10.1029/2007JD009682, 2008. 3178
- Preusse, P., Ern, M., Bechtold, P., Eckermann, S. D., Kalisch, S., Trinh, Q. T., and Riese, M.: Characteristics of gravity waves resolved by ECMWF, *Atmos. Chem. Phys.*, 14, 10483–10508, doi:10.5194/acp-14-10483-2014, 2014. 3175, 3176, 3182, 3199, 3200, 3202
- Sato, K., Watanabe, S., Kawatani, Y., Tomikawa, Y., Miyazaki, K., and Takahashi, M.: On the origins of mesospheric gravity waves, *Geophys. Res. Lett.*, 36, L19801, doi:10.1029/2009GL039908, 2009. 3175, 3182, 3183, 3202
- Sato, K., Tateno, S., Watanabe, S., and Kawatani, Y.: Gravity wave characteristics in the Southern Hemisphere revealed by a high-resolution middle-atmosphere general circulation model, *J. Atmos. Sci.*, 69, 1378–1396, doi:10.1175/JAS-D-11-0101.1, 2012. 3175, 3176, 3181, 3182, 3183, 3184, 3185, 3198, 3202
- Savitzky, A. and Golay, M. J. E.: Smoothing and differentiation of data by simplified least squares procedures, *Anal. Chem.*, 36, 1627–1639, 1964. 3179
- Scaife, A., Butchart, N., Warner, C., Stainforth, D., Norton, W., and Austin, J.: Realistic quasi-biennial oscillations in a simulation of the global climate, *Geophys. Res. Lett.*, 27, 3481–3484, doi:10.1029/2000GL011625, 2000. 3176
- Stockwell, R., Mansinha, L., and Lowe, R. P.: Localization of the complex spectrum: the S-Transform, *IEEE T. Signal Proces.*, 44, 998–1001, 1996. 3195

The southern stratospheric gravity wave hot spot

N. P. Hindley et al.

Title Page

Abstract

Introduction

Conclusions

References

Tables

Figures



Back

Close

Full Screen / Esc

Printer-friendly Version

Interactive Discussion



- Tsuda, T., Lin, X., Hayashi, H., and Noersomadi: Analysis of vertical wave number spectrum of atmospheric gravity waves in the stratosphere using COSMIC GPS radio occultation data, *Atmos. Meas. Tech.*, 4, 1627–1636, doi:10.5194/amt-4-1627-2011, 2011. 3177, 3186, 3189
- Wang, L. and Alexander, M. J.: Global estimates of gravity wave parameters from GPS radio occultation temperature data, *J. Geophys. Res.*, 115, D21122, doi:10.1029/2010JD013860, 2010. 3192, 3201
- Watanabe, S., Kawatani, Y., Tomikawa, Y., Miyazaki, K., Takahashi, M., and Sato, K.: General aspects of a T213L256 middle atmosphere general circulation model, *J. Geophys. Res.*, 113, D12110, doi:10.1029/2008JD010026, 2008. 3176, 3181, 3183, 3202
- Wright, C. J. and Gille, J. C.: Detecting overlapping gravity waves using the S-Transform, *Geophys. Res. Lett.*, 40, 1850–1855, doi:10.1002/grl.50378, 2013. 3188, 3189, 3195
- Wright, C. J., Osprey, S. M., and Gille, J. C.: Global observations of gravity wave intermittency and its impact on the observed momentum flux morphology, *J. Geophys. Res.-Atmos.*, 118, 10980–10993, doi:10.1002/jgrd.50869, 2013. 3190
- Wu, D. L. and Jiang, J. H.: MLS observations of atmospheric gravity waves over Antarctica, *J. Geophys. Res.*, 107, 4773, doi:10.1029/2002JD002390, 2002. 3175
- Wu, D. L. and Waters, J. W.: Satellite observations of atmospheric variances: a possible indication of gravity waves, *Geophys. Res. Lett.*, 23, 3631–3634, doi:10.1029/96GL02907, 1996. 3175, 3181
- Yan, X., Arnold, N., and Remedios, J.: Global observations of gravity waves from High Resolution Dynamics Limb Sounder temperature measurements: a year-long record of temperature amplitude, *J. Geophys. Res.*, 115, D10113, doi:10.1029/2008JD011511, 2010. 3175, 3181

The southern stratospheric gravity wave hot spot

N. P. Hindley et al.

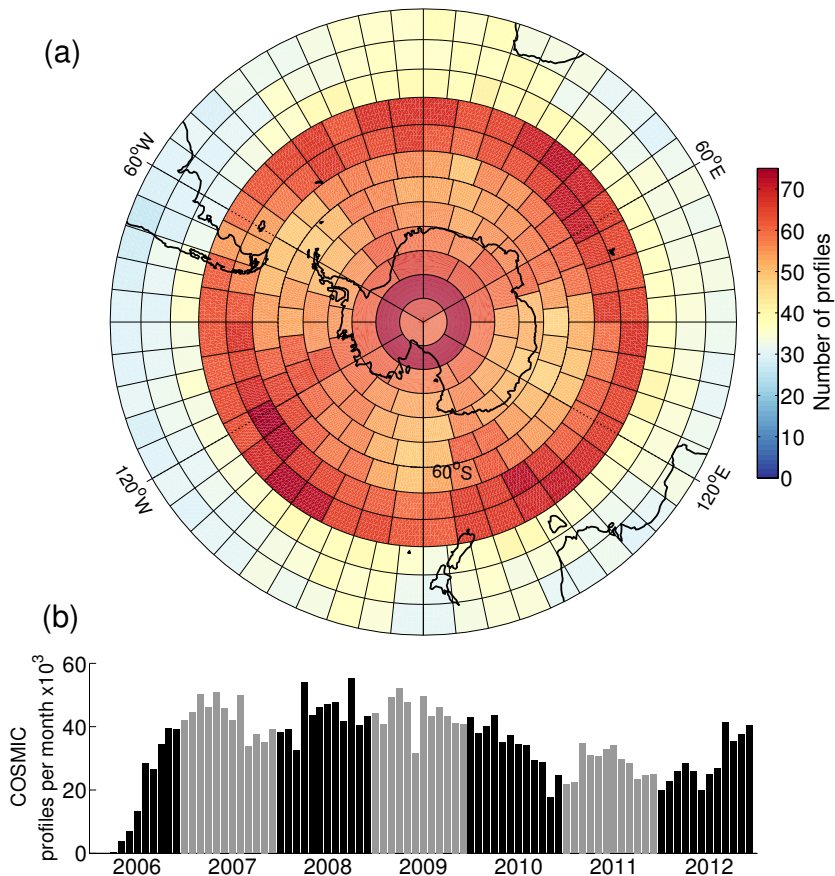


Figure 1. Polar stereographic projection of monthly-mean COSMIC sampling density for the period 2007–2012 (a), and total number of occultations per month for the period 2006–2012 (b). Each box in (a) represents an equal area of approximately 550 km². Alternating years in (b) are shown by black and gray bars.

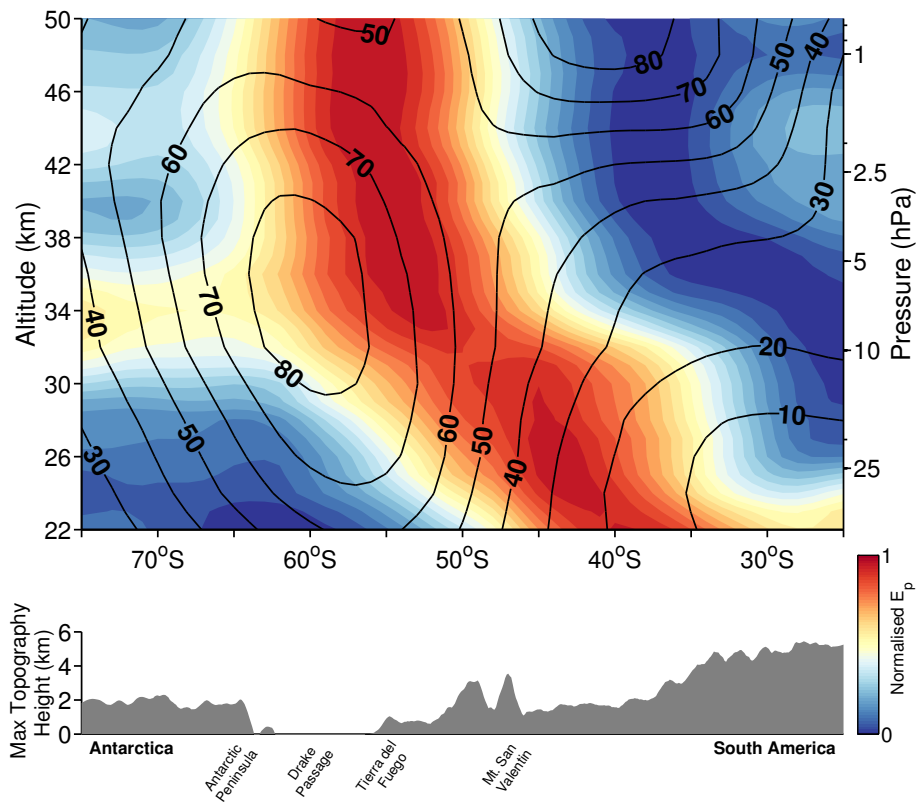


Figure 3. Normalised monthly-mean meridional cross-section of E_p in August 2010 over the southern Andes and Antarctic Peninsula (top panel) and maximum topography height (bottom panel) in a $\pm 5^\circ$ slice centred on 65° W. Monthly-mean zonal-mean winds from ECMWF operational analyses are shown by thick contours in the top panel, at intervals of 10 ms^{-1} . Note the E_p has been normalised at each height level to highlight the vertical structure.

The southern stratospheric gravity wave hot spot

N. P. Hindley et al.

Title Page

Abstract Introduction

Conclusions References

Tables Figures

◀ ▶

◀ ▶

Back Close

Full Screen / Esc

Printer-friendly Version

Interactive Discussion



The southern stratospheric gravity wave hot spot

N. P. Hindley et al.

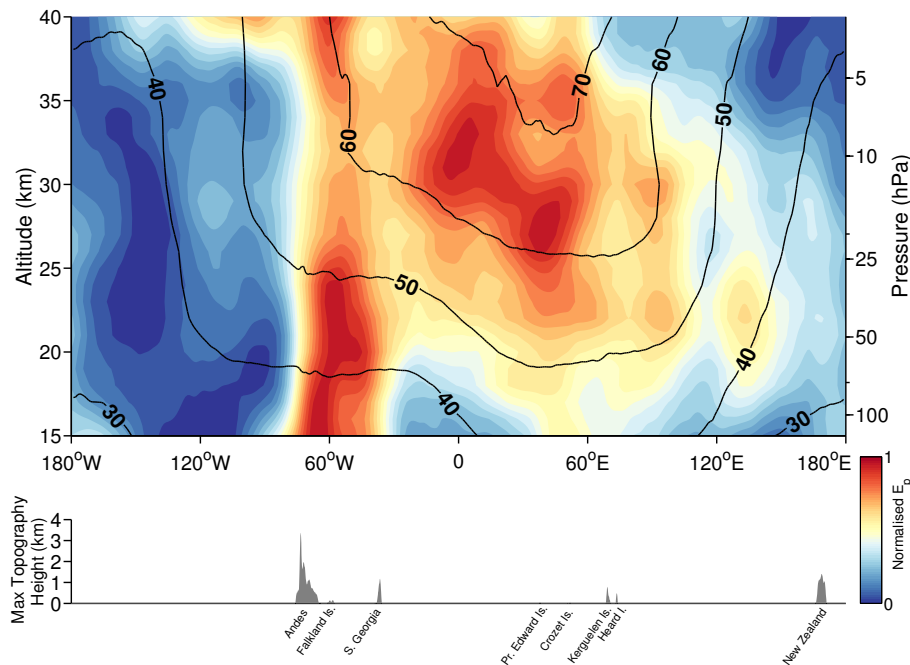


Figure 4. Normalised monthly mean zonal cross-section of E_p for August 2010 over Southern Ocean (top panel) and maximum topography height (bottom panel) in a $\pm 10^\circ$ slice centred on 50° S. Monthly mean zonal mean winds from ECMWF operational analyses are shown by thick contours in the top panel, at intervals of 10 ms^{-1} . Note the E_p has been normalised at each height level to highlight the vertical structure.

Title Page

Abstract

Introduction

Conclusions

References

Tables

Figures



Back

Close

Full Screen / Esc

Printer-friendly Version

Interactive Discussion



The southern stratospheric gravity wave hot spot

N. P. Hindley et al.

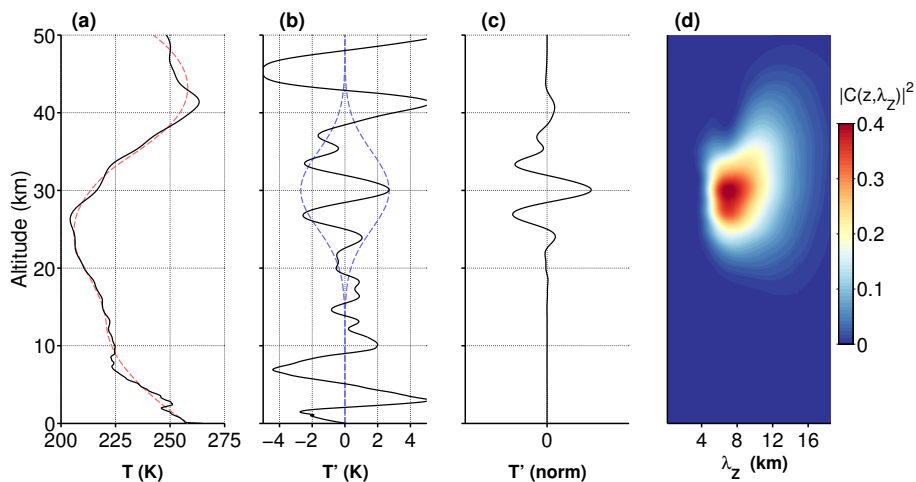


Figure 5. Processing chain for wave identification in a COSMIC profile at 23:19 UTC on 1 August 2010 at 53° S, 50° W. Panels show (a) raw temperature profile (black solid) and filtered background temperature profile (red dashed), (b) temperature perturbation profile (black solid) and Gaussian window centred on 30 km (blue dashed), (c) root-sum-square normalised and windowed perturbation profile, (d) squared covariance spectrum of the CWT of the profile in (c). For details, see text.

Title Page

Abstract

Introduction

Conclusions

References

Tables

Figures

◀

▶

◀

▶

Back

Close

Full Screen / Esc

Printer-friendly Version

Interactive Discussion



The southern stratospheric gravity wave hot spot

N. P. Hindley et al.

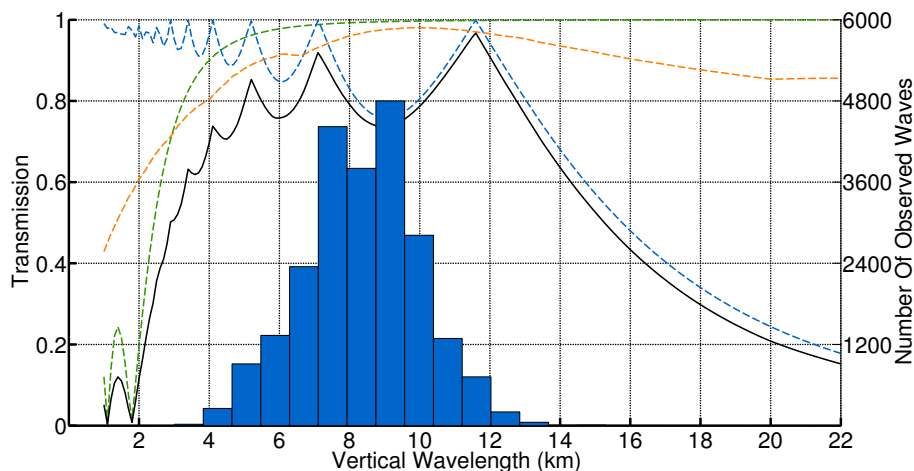


Figure 6. Transmission against vertical wavelength for each step in our Wave-ID processing for synthetic waves with $\lambda_z < 22$ km centred at 30 km altitude: background subtraction (blue dashed); noise reduction (green dashed); Gaussian windowing and CWT (orange dashed); and the combined transmission (black solid). Blue bars show a histogram (right axis) of number of waves identified in COSMIC data in the region 35–75° S 0–90° W during June–August 2006–2012 using this method.

Title Page

Abstract

Introduction

Conclusions

References

Tables

Figures



Back

Close

Full Screen / Esc

Printer-friendly Version

Interactive Discussion



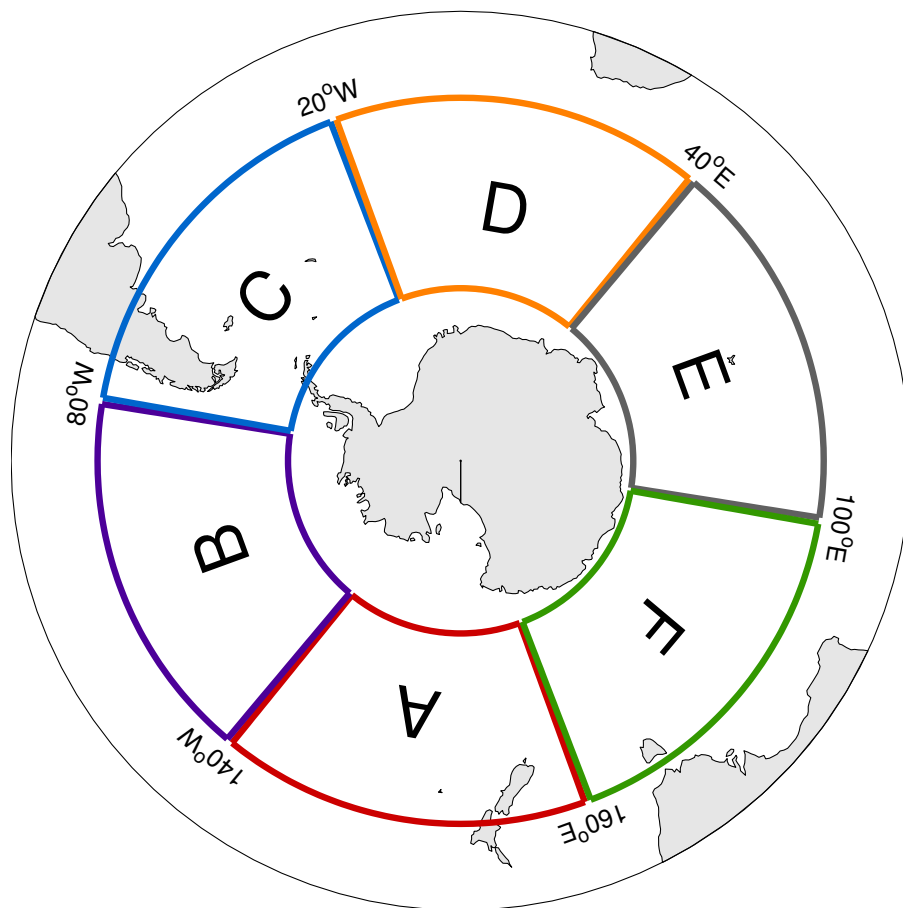


Figure 8. Polar stereo projection showing longitudinal Sectors A–F in the latitude band 40–65° S used in Fig. 9.

The southern stratospheric gravity wave hot spot

N. P. Hindley et al.

Title Page

Abstract Introduction

Conclusions References

Tables Figures

◀ ▶

◀ ▶

Back Close

Full Screen / Esc

Printer-friendly Version

Interactive Discussion



The southern stratospheric gravity wave hot spot

N. P. Hindley et al.

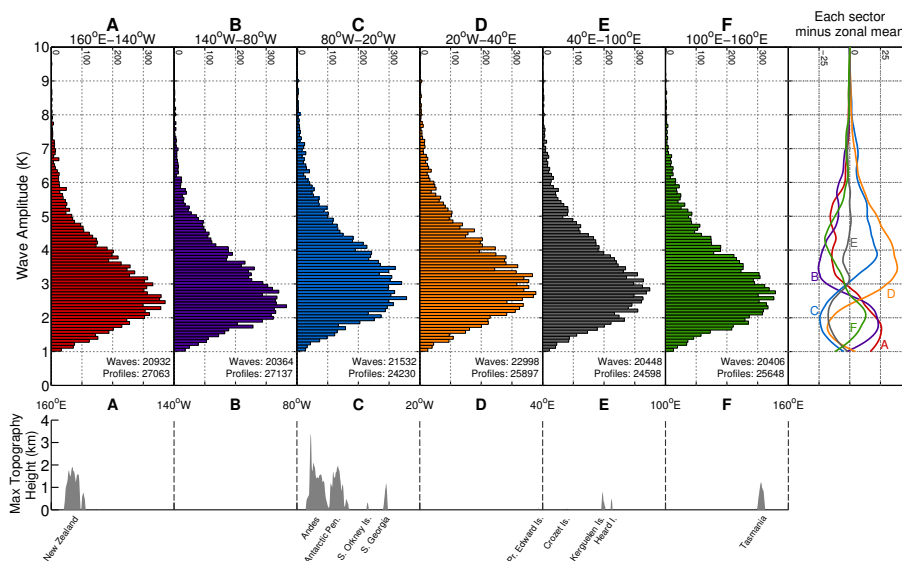


Figure 9. Histograms of individual wave amplitudes detected during June–August 2006–2012 in longitudinal Sectors A–F in the latitude band 40–65° S using the Wave-ID method (see text). The rightmost panel shows the difference between the wave amplitude distribution in each sector and the zonal-mean distribution. The bottom panel shows maximum topography height in the latitude band 40–65° S

Title Page

Abstract

Introduction

Conclusions

References

Tables

Figures

◀

▶

◀

▶

Back

Close

Full Screen / Esc

Printer-friendly Version

Interactive Discussion



The southern stratospheric gravity wave hot spot

N. P. Hindley et al.

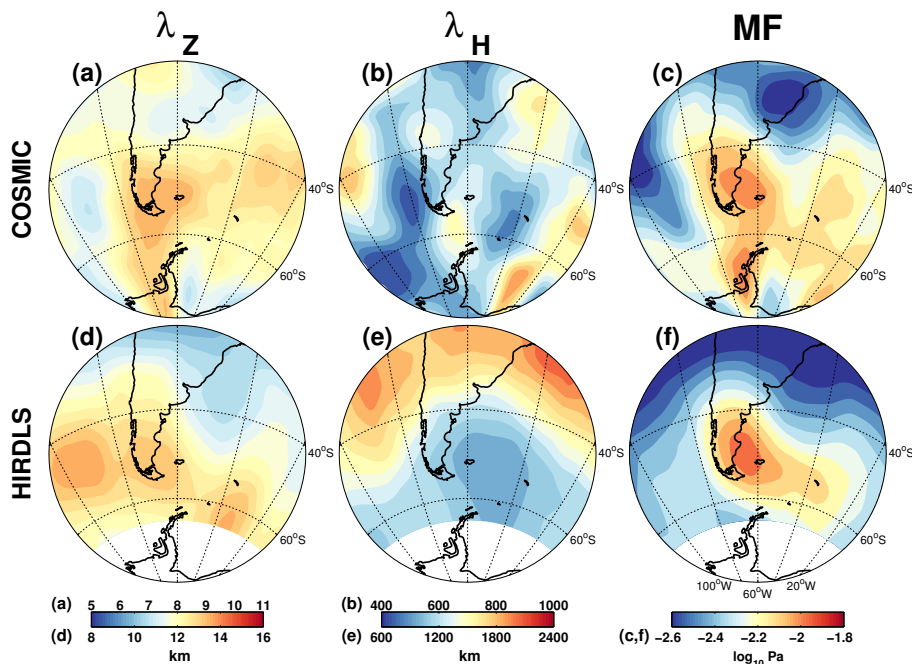


Figure 10. Orthographic projections of vertical wavelength λ_z , horizontal wavelength λ_H and momentum flux (MF) for COSMIC (a–c) and HIRDLS (d–f) at 30 km (~ 10 hPa) during June–August 2006.

Title Page

Abstract

Introduction

Conclusions

References

Tables

Figures

◀

▶

◀

▶

Back

Close

Full Screen / Esc

Printer-friendly Version

Interactive Discussion

